Sustainable H2 generation via steam reforming of biogas in membrane reactors: H2S effects on membrane performance and catalytic activity

Adolfo Iulianelli, Matteo Manisco, Nicolas Bion, Anthony Le Valant, Florence Epron, Ozgur Colpan, Elisa Esposito, John C Jansen, Mario Gensini, Alessio Caravella

Sustainable H_2 generation via steam reforming of biogas in membrane reactors: H_2S effects on membrane performance and catalytic activity

A. Iulianelli[1*], M. Manisco[1,2], N. Bion[3], A. Le Valant[3], F. Epron[3], C.O. Colpan[4], E. Esposito[1], J.C. Jansen[1], M. Gensini[1], A. Caravella[2]

[1] Institute on Membrane Technology - Italian National Research Council - via P. Bucci 17/C, Rende (CS), 87036, Italy
[2] DIMES Dpt. of University of Calabria, via P. Bucci 34/B, Rende (CS), 87036, Italy
[3] Institut de Chimie des Milieux et Matériaux de Poitiers(IC2MP), Université de Poitiers, CNRS, SAMCat, 4 rue Michel Brunet - B27 - TSA 51106, 86073 Poitiers Cedex 9, France
[4] Mechanical Eng. Dpt. of the Dokuz Eylul University, Tinaztepe Yerleskesi Buca, Izmir, 35397, Turkey

(*) Correspondence to: a.iulianelli@itm.cnr.it (Dr. Adolfo Iulianelli)

Abstract

This study proposes as first time the steam reforming of a synthetic biogas stream containing 200 ppm of H_2S, carried out in a non-commercial supported Pd-Au/Al_2O_3 membrane (7-8 μm of selective layer) reactor at 823 K and 150 kPa over a non-commercial Rh(1%)/$MgAl_2O_4$/Al_2O catalyst, recovering almost 80% of the total hydrogen produced during the reaction and showing a good resistance to the H_2S contamination as confirmed by stable methane conversions for around 400 h under operation. For comparison, the same reaction was carried out in a commercial self-supported Pd-Ag membrane (150 μm of wall thickness) yielding a hydrogen recovery equal to 40% at 623 K and 200 kPa and presenting stable methane conversions for less than 200 h under operation due to the effect of the H_2S contamination.

Keywords: Pd-Au/Al_2O_3 membrane, membrane reactor, hydrogen, Rh-based catalyst, biogas steam reforming

1. Introduction

Today, the general interest on ever more sustainable processes in strategic areas such as energy, environmental protection, etc. is involving a critical challenge represented by the transition from a fossil fuel-based to a sustainable and circular economy [1,2], adopting the principles of Process Intensification Strategy

to drive the transition from conventional to alternative and environmentally friendly technologies [3]. The concepts of this new strategy are well-matched by the membrane engineering, which is playing a crucial role in the substitution of a number of traditional devices used in the process engineering with membrane-based units such as the membrane reactors (MRs) [4,5].

As a consequence of the growing interest toward the so-called hydrogen economy [6], in the last decades, hydrogen production and purification technologies have attracted considerable interest and, among them, MR technology received growing attention, because able to combine the exploitation of renewable sources [7-10] with the simultaneous production and purification of hydrogen via reforming reactions [11-15]. In a MR, the presence of a hydrogen perm-selective membrane allows its selective removal from the reaction toward the permeate side, involving the so-called "shift-effect" on the reaction system, responsible for higher reaction products formation and further feed product conversion than an equivalent conventional reformer (CR) (for thermodynamically restricted reactions) [16].

To date, most of the production of hydrogen at a larger scale comes from natural gas steam reforming reaction [17], which involves the exploitation of fossil fuels and the consequent formation of greenhouse gases (GHGs).

According to the standard ISO 14001:2015 Environmental Management, any change to the environment, whether adverse or beneficial, wholly or partially resulting from an organization's environmental aspects should be considered [18]. Hence, a steam reforming plant, both classical and MR based, has an anthropogenic impact on the environment [19].

Among the renewable feedstocks, biogas results to be a greener option than the natural gas for generating hydrogen by reforming processes, ~~which may~~ contributing to lower the emission of GHGs [20]. The composition of biogas may vary greatly, depending on the nature of the residual biomass (sewage treatment plants, animal waste, etc.) used during the anaerobic digestion process, even though it is mostly constituted of CH_4 and CO_2, besides N_2, hydrogen, volatile organic compounds, H_2S, etc. [21,22]. However, the combination of biogas processing with MR technology was not largely studied in the literature, particularly because of the presence of H_2S as main responsible for the membrane and catalyst poisoning and consequent

performance loss. However, in the last years, there has been a growing attention toward the development of high performance reforming catalysts, showing high catalytic activity, high carbon deposition resistance, etc. According to the specialized literature, metal catalysts such as Rh, Pd or Ru, Pt, and Ni, showing high activity and selectivity, were used for hydrogen generation via steam reforming of biogas (SRB) [23]. To date, most of the scientific literature about the SRB reaction in CRs is based on Ni catalysts, even though Rh presents a greater catalytic activity than Ni, associated to a lower coke formation tendency [24-28]. The choice of the support is also of major importance since it plays an essential role in the stability of the catalyst. In the last years, it was experienced that catalysts constituted of Rh supported on γ-Al_2O_3 modified by cations such as Mg^{2+} were efficient for steam reforming reactions [29,30]. On the other hand, only a few studies deal with the utilization of Pd-based MRs to carry out the steam reforming of a real or synthetic biogas stream. In these studies, both fluidized bed [31,37] and packed bed [32-36,38,39] MR modalities were analyzed with the purpose of producing high grade hydrogen using synthetic H_2S free biogas mixtures [31-34], or considering a pre-treatment step useful to remove H_2S prior to the reforming stage [40-42]. In particular, Ru/Al_2O_3 catalyst and a thick self-supported Pd-Ag membrane (200 μm) were used by Itoh's group [32,33], while Ni-based catalysts were packed in self-supported Pd-Ag [38,39] and supported Pd (7 μm layer)/Al_2O_3 MRs [36]. To the best of our knowledge, in only one case a commercial Rh-based catalyst was used in a fluidized bed MR housing a supported Pd-Ag (5 μm layer)/Al_2O_3 membrane [31].

According to what stated above, pure Pd membranes suffer a lot the H_2S attack, which is responsible for the block of the H_2 dissociation sites and, in some case, for the formation of the Pd_4S in the membrane bulk, causing ~~with the consequent their~~ the performance loss due to the lower hydrogen permeability of Pd_4S than pure Pd, or the membrane failure after long-term exposure [43-48]. On the contrary, Pd-Au and Pd-Cu alloyed membranes result to be more H_2S resistant than pure Pd ones [52-56]. In particular, the growing interest in Pd-Au alloy membranes has been due to their superior hydrogen permeability performance and higher resistance to H_2S poisoning with respect to Pd-Cu membranes [56]. For example, Chen and Ma [44] performed H_2 permeation tests on a Pd-Au membrane in presence of ~ 55 ppm of H_2S at 773 K and 200 kPa, founding that higher temperatures allowed quicker hydrogen recovery when H_2S was removed, whereas

longer H_2S exposure determined longer hydrogen recovery times. Coulter et al. [49] tested Pd-Au membrane foils under permeation tests of hydrogen-rich syngas streams containing from 20 to 50 ppm of H_2S at 673 K and 1253 kPa, at different Au compositions (between 7 and 20 wt%), observing that higher Au content in the alloy determined a lower H_2S inhibition effect on the H_2 permeability. The most recent research focuses on Pd-ternary alloys (among Pd, Au, Pt, Ag etc.) membranes, although their fabrication and testing result to be at an infancy stage [43,49,54,56]. In some case, Pd-ternary alloys membranes showed very good tolerance toward H_2S (up to 1000 ppm) during hydrogen permeation tests, without a clear evidence of performance loss due to the Pd_4S formation [54].

The aim of this experimental study is to perform the steam reforming of a synthetic biogas mixture containing H_2S in two MRs: the first, housing a high hydrogen permeable and low hydrogen perm-selective supported Pd-Au/Al_2O_3 membrane; and the second, housing a low hydrogen permeable and high hydrogen perm-selective self-supported Pd-Ag membrane. Both the MRs are packed with a non-commercial Rh(1%)/$MgAl_2O_4$/Al_2O catalyst. In our previous studies, Pd-Au membranes supported on ceramic [57] and porous stainless steel [58] supports were studied in terms of hydrogen permeation characteristics at different experimental conditions, analyzing the role of the presence/absence of an intermediate layer between the separative metallic layer and the support, without evaluating the effect of the contaminants presence such as H_2S in the feed stream. Furthermore, a H_2S-free synthetic biogas stream was used to produce high grade hydrogen via steam reforming reaction performed in a Pd/Al_2O_3 MR [36].

The novelty of this study consists in evaluating the effects of the H_2S, presence in the model biogas stream, on the catalytic activity and the hydrogen perm-selectivity characteristics of the Pd-alloyed membranes. As stated above, the effect of H_2S contained in hydrogen-rich feed streams during the hydrogen permeation through Pd-Au membranes was investigated by a number of scientific papers, but to our best knowledge no papers deal with the steam reforming of a H_2S-containing biogas stream carried out in a Pd-Au based MR, where the effects of the simultaneous presence of H_2S, CO_2 and other reaction byproducts were evaluated in terms of hydrogen permeation membrane performance and catalytic activity as well. Furthermore, an

equivalent H_2S free biogas mixture is used for better highlighting the role of H_2S during the SRB on the MRs performance, evaluated in terms of methane conversion, hydrogen recovery and purity.

2. Experimental

2.1 Catalyst preparation and characterization

The experimental campaign was performed using a Rh(1%)/$MgAl_2O_4$/Al_2O catalyst. The catalyst support was constituted of γ-alumina beads (200 m^2g^{-1}, 1-2 mm in diameter, provided by AXENS) impregnated with magnesium acetate ($Mg(CH_3COO)_2{\cdot}4H_2O$, Alpha Aesar) to achieve 5 wt.% of magnesium in the support [59]. The choice of the acetate was due to the better control of the acidic-base behaviors of the support. After impregnation, the support was subjected to various optimal thermal treatments, especially at high temperature (1273 K) in order to form the $MgAl_2O_4$ spinel structure at the outer shell of the alumina support [59]. Rh (1% wt), as metallic catalyst phase, was wet impregnated to the support by using $RhCl_3$ (Alpha Aesar) for 4 h at room temperature. After impregnation procedure, the catalyst was placed under stirring at 318 K for 24 h and dried at 393 K for 15 h. Then, it was activated by calcination at 973 K for 4 h (heating ramp 295 K min^{-1}).

The bare alumina beads, the alumina modified by the addition of magnesium and thermal treatment and Rh/$MgAl_2O_4$/Al_2O_3 catalyst were characterized by nitrogen adsorption (Micromeritics Tristar 3000) for the determination of the BET surface area, hydrogen chemisorption for the determination of the metal accessibility, ICP-OES (Perkin-Elmer Optima 2000 DV) for the metal content, X-Ray Diffraction (Siemens D5000) and Scanning Electron Microscopy (INCA 300 OXFORD).

2.2 Membranes characterization and testing

The non-commercial supported Pd-Au/α-Al_2O_3 membrane (Nanjing Tech. University & GaoQ Functional Materials Co., Ltd., China) is constituted of a thin Pd-Au layer (~ 8 µm) deposited on the porous substrate (α-Al_2O_3) via electroless plating technique and the total membrane length is 7.5 cm, with 5.0 cm of active length, o.d. 13 mm and i.d. 8 mm, Figure 1(a).

Chemical and morphological analyses were performed by scanning electron microscopy (Phenom Pro X desktop SEM, Phenom-World), which is equipped with an energy dispersive X-ray spectroscopy detector (EDX) allowing elemental analysis of membrane surface and cross-section before and after (post mortem analysis) the experimental campaign.

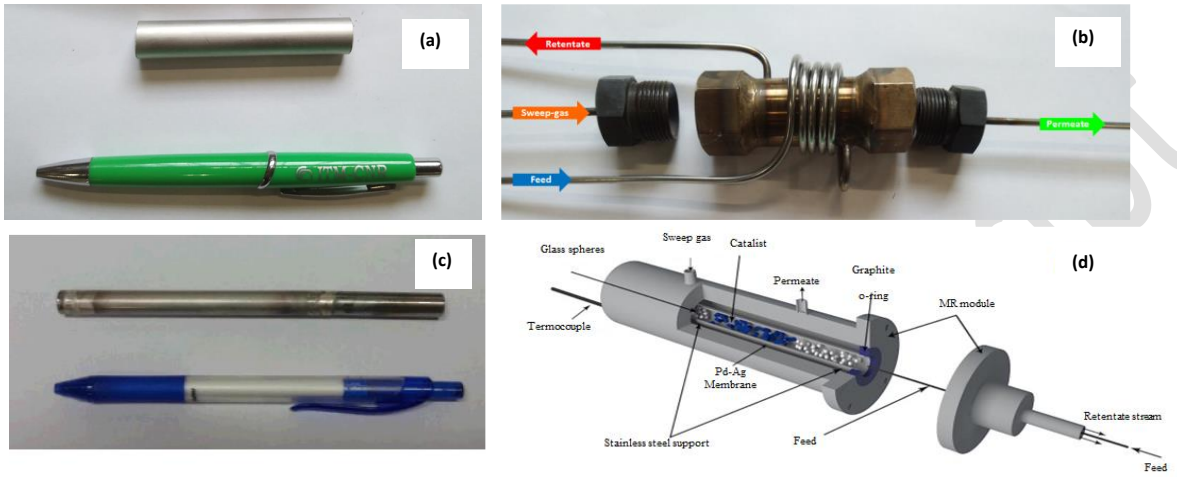

Figure 1. Photos of the (a) supported Pd-Au/α-Al_2O_3 membrane before the experimental tests; (b) bench-scale tubular MR module; (c) photo of the self-supported Pd-Ag membrane; (d) scheme of the Pd-Ag MR.

The bench-scale Pd-Au/Al_2O_3 MR module is illustrated in Figure 1(b), in which the feed, sweep-gas, retentate and permeate streams are clearly shown. The MR module is 12 cm in total length and 3.0 cm of o.d. and the supported Pd-Au based membrane is housed inside by using two graphite gaskets useful to prevent the mixing within permeate and retentate streams. The Rh-based catalyst (1.5 g) was packed in the annulus of the MR, while the permeated products were collected in the lumen of the MR for successive gas chromatograph (GC) analyses.

The commercial self-supported Pd-Ag membrane (Johnson Matthey, UK) is constituted of a wall thickness of about 150 µm, o.d. 10 mm, 145 mm as total length, and 100 mm as active length, Figure 1(c). In this study, the Pd-Ag membrane is closed at one end and the catalyst is packed in the lumen side, Figure 1(d). Before the reaction tests, the Rh-based catalyst was reduced under pure hydrogen for 1 h. The MR was heated up by using an electrical heating tape connected to a temperature controller and a thermocouple. The experimental campaign started with single gas (H_2, N_2, CO_2, CH_4) permeation tests, performed between 573 and 823 K, by varying the feed pressure between 150 and 250 kPa (abs.). Afterwards, the SRB reaction was

carried out in the MRs with the temperature varying between 673 and 823 K and the pressure between 150 kPa (abs.) and 250 kPa (abs.), by means of a back-pressure controller (Fantinelli, Italy) placed at the outlet side of the retentate stream. The H_2O/CH_4 feed molar ratio was set at 2/1 and 3/1, and two synthetic biogas mixtures (with and without H_2S) flowed into the MRs. The composition of the gas mixture for both cases is given in Table 1. The weight hourly space velocity (WHSV) was varied during the reaction tests from 0.2 to 1.3 h^{-1}.

Table 1. Synthetic biogas mixtures used during the experimental reaction tests (molar percentages).

Compound	Mixture 1 (with H_2S) [%]	Mixture 2 (H_2S free) [%]
CO_2	35.03	35.00
CH_4	59.94	60.00
N_2	5.01	5.00
H_2S	0.02	-

In the experimental setup, deionized water for the SRB reaction, which was vaporized in a preheating zone and, then, mixed with the synthetic biogas mixture, was fed by a P680 HPLC pump (Dionex). The outlet streams were cooled by a cold-trap to condensate the unreacted steam and, hence, analyzed by a temperature-programmed HP 6890 GC, equipped with two thermal conductivity detectors at 523 K and using Ar as a carrier gas. The GC was equipped by three packed columns: Porapack R 50/80 (8 ft $\times$ 1/8 inch) and Carboxen™ 1000 (15 ft $\times$ 1/8 inch) connected in series, and a Molecular Sieve 5 Å (6 ft $\times$ 1/8 inch). Furthermore, a constant flow rate of N_2 (~ 25 mL/min) was used as an internal standard gas to analyze the outlet compositions (dry state) of both permeate and retentate streams. Both single gases (CH_4, CO_2, N_2, H_2) and mixtures were supplied by means of Brooks Instruments 5850S mass-flow controllers, driven by the Lira (Italy) software. Each experimental reaction data of this work represents an average value of – at least – 5 experimental tests taken in 150 min at the steady-state condition with an error variation lower than 2% for each experimental point reported in this work. The performance of the MRs during SRB reaction was evaluated by means of the following definitions:

$$\text{Methane conversion}(\%) = \frac{CH_{4\text{-in}} - CH_{4\text{-out}}}{CH_{4\text{-in}}} \times 100 \quad (1)$$

where $CH_{4\text{-in}}$ and $CH_{4\text{-out}}$ are the inlet and outlet CH_4 molar flow rates, respectively.

$$\text{Hydrogen recovery (\%)} = \frac{H_{2-\text{permeate}}}{(H_{2-\text{permeate}} + H_{2-\text{retentate}})} \times 100 \quad (2)$$

where $H_{2\text{-permeate}}$ and $H_{2\text{-retentate}}$ are the outlet H_2 molar flow rates in the permeate and retentate sides, respectively.

$$\text{Hydrogen permeate purity (\%)} = (H_{2\text{-permeate}}/F_{\text{permeate}}) \times 100 \quad (3)$$

where F_{permeate} represents the outlet permeate molar flow rate. Furthermore, to analyze the permeation behaviours of the Pd-Au/Al_2O_3 and Pd-Ag membranes, single gas permeation tests were done according to the following general equation, regulating the H_2 flux permeating through a generic membrane:

$$J_{H_2} = Pe(p^n_{H2\text{-retentate}} - p^n_{H2\text{-permeate}}) \quad (4)$$

where J_{H2} indicates the H_2 flux permeating through the membrane, Pe is the H_2 permeance, $p_{H2\text{-retentate}}$ and $p_{H2\text{-permeate}}$ are the H_2 partial pressures in the retentate and permeate sides, respectively, and n (variable in the range 0.5 - 1) is the dependence factor of the H_2 permeating flux on the H_2 partial pressure;

$$\alpha_{H2/i} = \frac{J_{H2}}{J_i} \quad (5)$$

where $\alpha_{H2/i}$ represents the "ideal selectivity", calculated as the ratio within the hydrogen permeating flux (J_{H2}) over the permeating flux of another pure gas (J_i, with i = CO_2, CH_4, and N_2). The correlation between the H_2 membrane permeability (P_{H2}) and the temperature was described by an Arrhenius-like equation (Eq. 6).

$$P_{H2} = P_{H2,0} exp^{(-\frac{E_A}{RT})} \quad (6)$$

where $P_{H2,0}$ represents the pre-exponential factor, R is the universal gas constant, E_A is the apparent activation energy and T is the temperature.

3. Results and Discussion

3.1. Characteristics of the Rh/$MgAl_2O_4$/Al_2O_3 catalyst for reforming reaction

X-Ray diffractograms of the bare alumina support, of the alumina modified by Mg^{2+} and of the Rh/$MgAl_2O_4$/Al_2O_3 catalyst are displayed in Figure 2(a). It can be seen that the impregnation of the magnesium precursor salt followed by a thermal treatment allows the incorporation of the Mg^{2+} cations into

the alumina support forming a magnesium aluminate phase, $MgAl_2O_4$, coexisting with an α-Al_2O_3 phase, with no trace of isolated Mg species, in accordance with the results of Aupretre et al. [59]. The SEM image of an alumina bead after modification by Mg^{2+} shows a core-shell structure with $MgAl_2O_4$ in the shell (thickness in the range of 190-210 μm) and a core of Al_2O_3. When rhodium is added, the diffractogram is similar to that of $MgAl_2O_4/Al_2O_3$ with no diffraction lines corresponding to Rh species indicating a good dispersion of Rh species on the support, Figure 2(b).

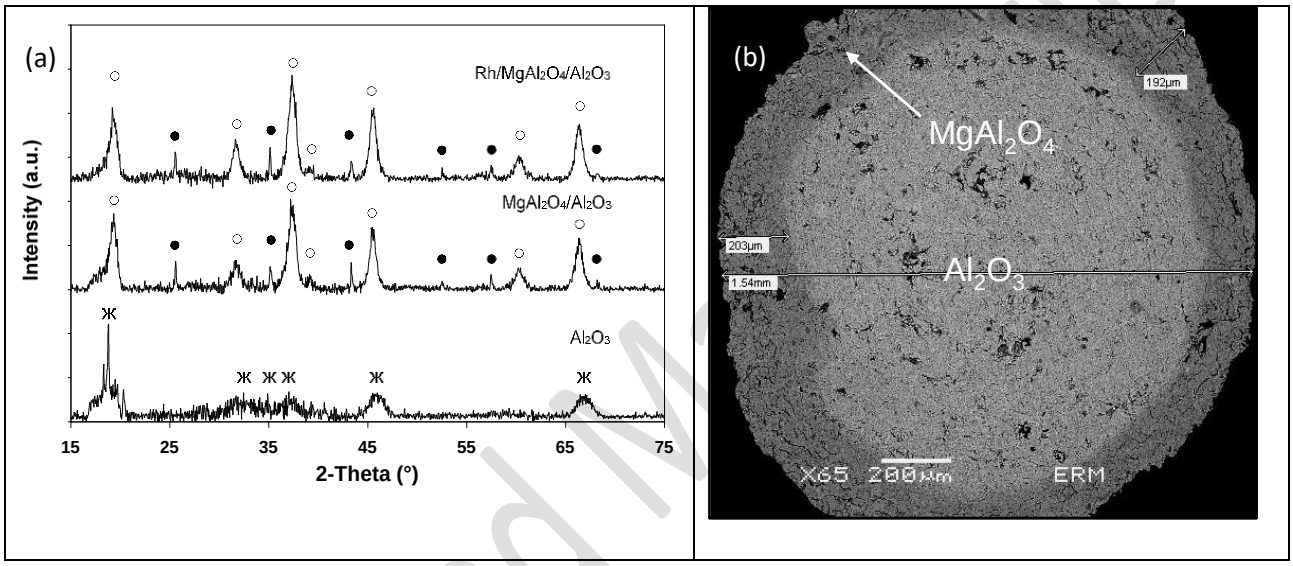

Figure 2. (a) X-Ray diffractograms of the alumina beads (Al_2O_3), the alumina beads modified by addition of Mg^{2+} ($MgAl_2O_4/Al_2O_3$) and the final catalyst (Rh/ $MgAl_2O_4/Al_2O_3$) (● : $MgAl_2O_4$, ○ : α-Al_2O_3 , ж : γ-Al_2O_3) and (b) SEM image of one bead of $MgAl_2O_4/Al_2O_3$.

The main characteristics of these materials are reported in Table 2. The thermal treatment at high temperature and the addition of Mg^{2+} induce a strong decrease of the BET surface area of the support from 207 $m^2\ g^{-1}$ for the bare alumina to 84 $m^2\ g^{-1}$ for while the addition of Rh does not modify the support. Rh and Mg contents are similar to the nominal values and the Rh dispersion of 40 wt% corresponding to Rh particle sizes of 2 nm considering hemispherical particles.

Table 2. Main characteristics of the studied catalyst.

Catalyst	BET surface area ($m^2\ g^{-1}$)	Rh content (wt.%)	Mg content (wt.%)	Rh dispersion[a] (%)
γ- Al_2O_3	207	-	-	-
$MgAl_2O_4/Al_2O_3$	84	-	4.6	-
$Rh(1\%)/MgAl_2O_4/Al_2O_3$	84	0.93	4.6	40

[a] determined from H_2 chemisorption measurements considering a stoichiometry H/Rh of 1

3.2 Experimental tests on the Pd-Au/Al_2O_3 membrane: gas permeation, SEM and EDX analyses

The first part of the whole experimental campaign of this work was devoted to analyzing the chemical-physical characteristics of the Pd-Au/Al_2O_3 membrane before the permeation and reaction tests.

Figures 3(a) and (b) show the Pd-Au/Al_2O_3 membrane, evidencing the characteristic cauliflower morphology of Pd-alloy layer at different magnification, respectively. Figure 3(c) illustrates the cross-section of the membrane from which the thickness of the dense metallic layer was estimated to be around 7-8 μm. Figure 3 (d) reports the porous Al_2O_3 support, where Pd was deposited with Au to constitute a thin dense layer well adhered to the former. The EDX analysis on this membrane confirmed the presence of the following atoms: Pd, Au, Al, O besides Si, Y and N as impurities, Figure 4.

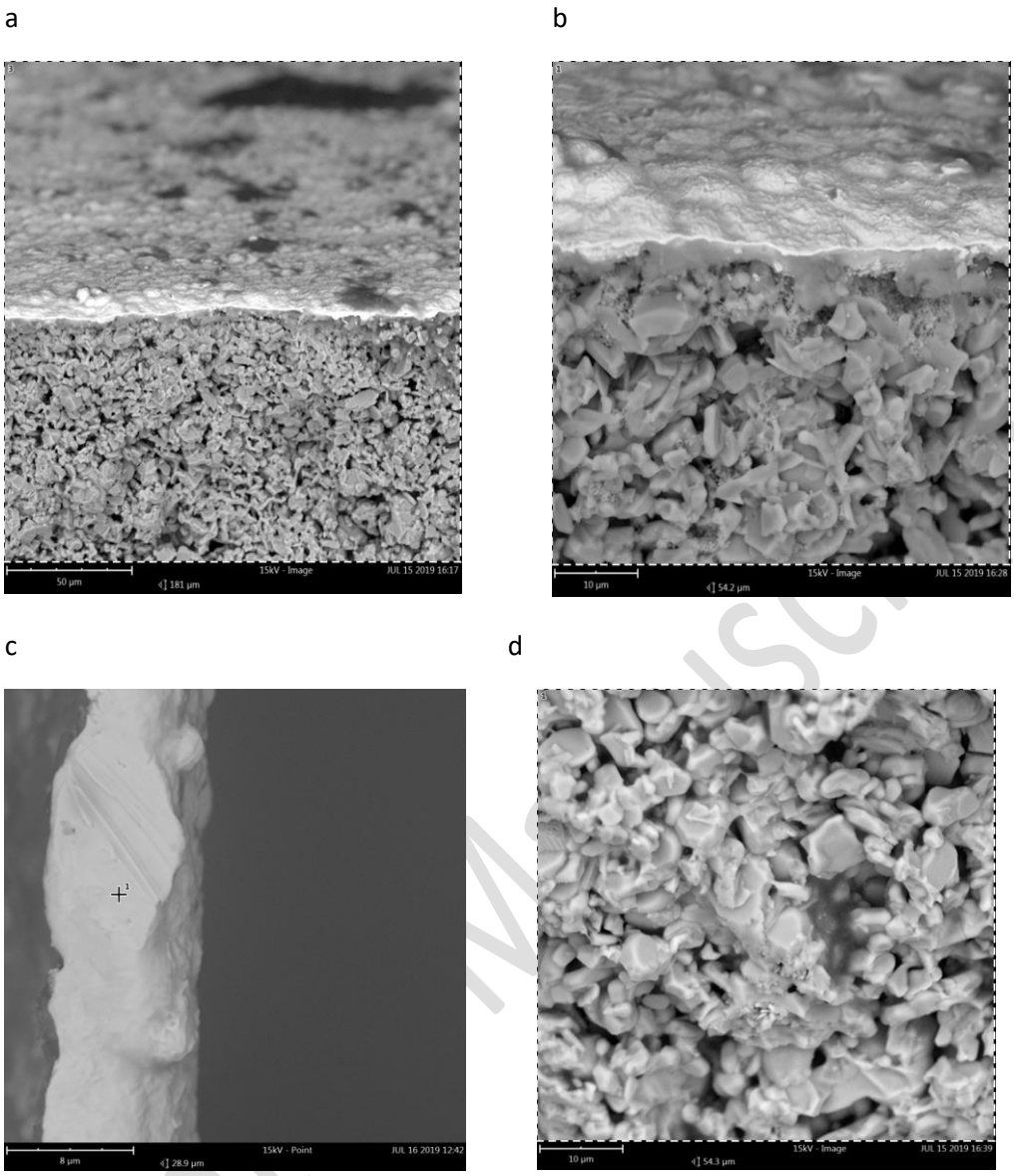

Figure 3. SEM images at different magnification of cross-section and surface of the Pd-Au/Al_2O_3 membrane at an accelerating voltage of 15 kV: a) and b) panoramic views of the membrane sample at different magnification; c) cross section; d) Al_2O_3 support.

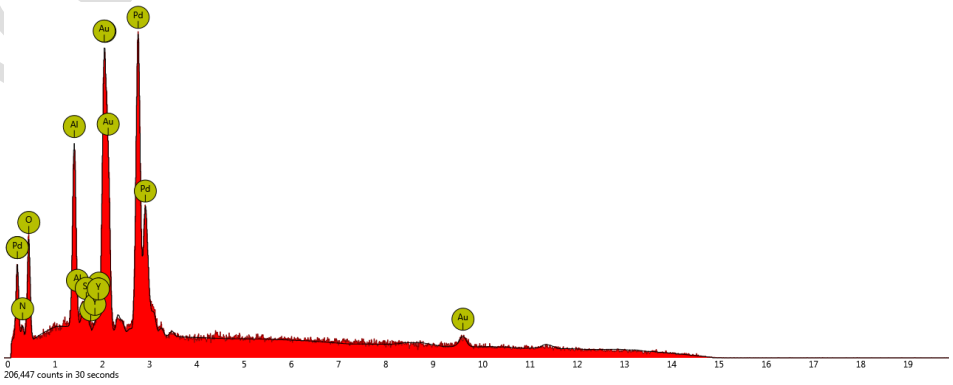

Figure 4. EDX analysis on the Pd-Au/Al_2O_3 membrane before the gas permeation and reaction tests.

Afterwards, single gas permeation tests were carried out on the Pd-Au/Al_2O_3 membrane in order to evaluate the H_2 perm-selectivity characteristics and the resistance to the effect of H_2S during the permeation test using the gaseous mixtures (Mixture 1 and Mixture 2) of Table 1. In particular, pure H_2 permeation tests were conducted between 573 and 823 K, varying the transmembrane pressure between 0 and 100 kPa, Figure 5(a).

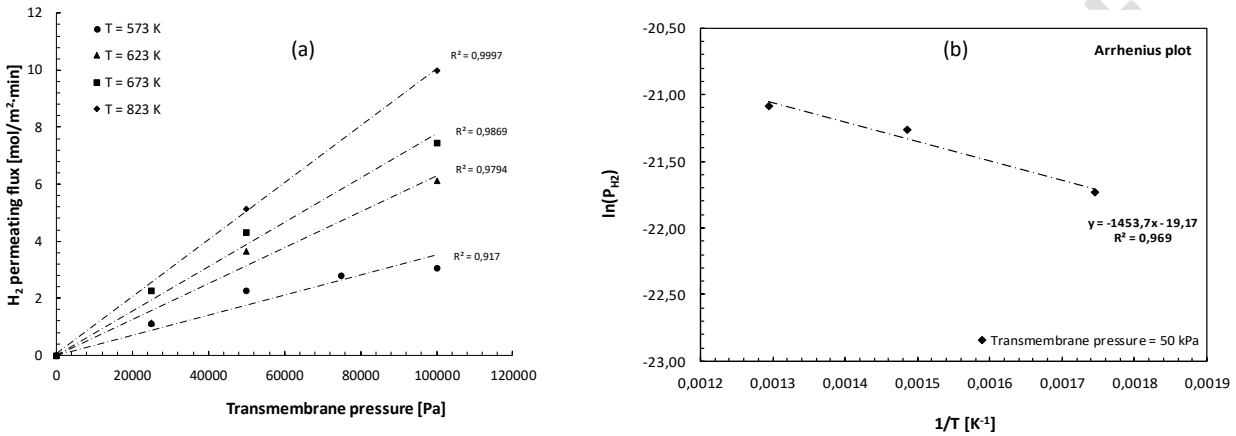

Figure 5. (a) H_2 flux permeating through the Pd-Au/Al_2O_3 membrane vs transmembrane pressure at different operating temperatures; (b) H_2 permeability vs 1/T for the Pd-Au/Al_2O_3 membrane at 50 kPa of transmembrane pressure.

As expected, the H_2 flux permeating through the membrane increased by raising the transmembrane pressure (as higher the transmembrane pressure as higher the H_2 permeation driving force) and the temperature. In particular, an increase of temperature allowed an enhancement of the H_2 permeating flux; indeed, the H_2 permeability depends on the temperature according to an Arrhenius-like equation, Figure 5(b) The apparent activation energy (E_A) was graphically estimated at 50 kPa of transmembrane pressure from the plot of Figure 5(b), which gives 12.1 kJ/mol with the correlation coefficient $R^2 \sim 0.97$, hence comparable to other literature data [60-68], Table 3.

Furthermore, a graphical assessment of the H_2 permeating flux plot as a function of the H_2 permeation driving force at different "n-value" was carried out. The "n" exponent of the hydrogen partial pressure represents the dependence factor of the H_2 flux permeating through the membrane on the H_2 partial pressure, and the regression factor (R^2) indicates when it achieves the maximum value, the best experimental data fitting.

Table 3. Comparison of the activation energy (E_A) of the Pd-Au/Al_2O_3 membrane with other literature data.

Metallic layer	Layer thickness (μm)	Substrate	Permeation T (K)	Δp (kPa)	E_A (kJ/mol)	Ref.
Pd-Cu	7	Al_2O_3-PNS [a]	813	2000	19.0	[60]
Pd-Cu	20	Al_2O_3	673	50	18.5	[61]
Pd-Au	5	YSZ [b]	623-823	100-700	7.5	[62]
Pd-Cu	17	PSS [c]	823	70	9.4	[63]
Pd-Ag	48	PSS [c]	623-823	180-250	9.0	[64]
Pd	15	Al_2O_3	623-923	30	10.0	[65]
Pd	7	Al_2O_3	623-723	100	11.4	[66]
Pd-Cu	10	ZrO_2/PSS [c]	713	-	15.4	[67]
Pd-HF	5	Al_2O_3	873	200	21.3	[68]
Pd-Au	8	Al_2O_3	673	50	12.1	**This work**

[a] Porous nickel support

[b] Yttria stabilized zirconia

[c] Porous stainless steel

Commonly, for thin metallic layers (< 5 μm) "n" may range between 0.5 and 1.0 and, when n = 0.5, the Eq. (4) describing the correlation between the H_2 permeating flux and H_2 permeation driving force becomes the Sieverts-Fick law, which means that the H_2 permeation depends substantially on the diffusion of atomic H_2 into the bulk [63]. The latter case results to be the rate-limiting step of the overall permeation process. On the other hand, when n = 1, Eq. (4) describes the H_2 permeation controlled by the mass transport to or from the surface or by the dissociative adsorption or associative desorption. When "n-value" ranges from 0.5 to 0.8, the H_2 permeation is regulated by different contributions such as diffusion, Knudsen, or viscous flow [69]. In Table 4, the n-values are reported as a function of temperature and each value of them represents the best data fitting (maximum R^2) at a set temperature.

Table 4. H_2 partial pressure exponent (n-value) at the maximum R^2 as a function of temperature for the Pd-Au/Al_2O_3 membrane.

T [K]	n-value
573	0.5
623	1.0
673	0.8
823	0.8

According to what was demonstrated by Caravella et al. [70] for membrane thickness (Pd-based layer) lower than 20 μm, the trend of n-value may show a maximum that, in this work, was reached at 623 K. Therefore, at a lower temperature, the H_2 permeation through the Pd-Au/Al_2O_3 membrane is controlled by the diffusion through the Pd-Au bulk, showing the best n-value is equal to the Sieverts coefficient (0.5). Increasing the temperature, the maximum R^2 was achieved at higher n-values. In particular, at 623 K, the best n-value was equal to 1, highlighting that the H_2 permeation is completely controlled by the surface mass transport. By increasing the temperature, the best n-value achieved a plateau around 0.8. This means that different mechanisms contribute to control the hydrogen permeation through this membrane. Afterwards, as a function of the operating time, the permeation of H_2 through the membrane was studied as a component in H_2-rich gas mixtures (a constant H_2 stream, 474 mL/min, mixed with a gaseous stream constituted of CO_2/CH_4/N_2 with and without H_2S, Table 5) and compared to that as single gas. This allowed to evaluate the eventual depletion of the H_2 permeating volume flow rate due to the effects of the concentration polarization, the adsorption of some components on the membrane surface, and - particularly - the harmful presence of H_2S.

Table 5. H_2-rich gas mixtures composition constituted of a constant H_2 stream, 474 mL/min, mixed with variable volume flow rates of gaseous streams constituted of CO_2/CH_4/N_2, with and without H_2S.

$Q_{TOT\text{-}mix\ gases}$ (*) [mL/min]	Q_{H2} [mL/min]	$Q_{TOT\ H2\text{-}rich\ mix}$ [mL/min]	$x_{H2\text{-}rich\ mix}$ [%]
26.4	474	500.4	95
54.6	474	528.6	90
11.8	474	586.8	81
173.4	474	647.4	73
294	474	768	62
666.6	474	1140.6	42

(*) Gaseous mixtures composition (without H_2);
a) with H_2S: CO_2(35.03%)/CH_4(59.94%)/N_2(5.01%)/H_2S(0.02%);
b) without H_2S: CO_2(35%)/CH_4(60%)/N_2(5%).

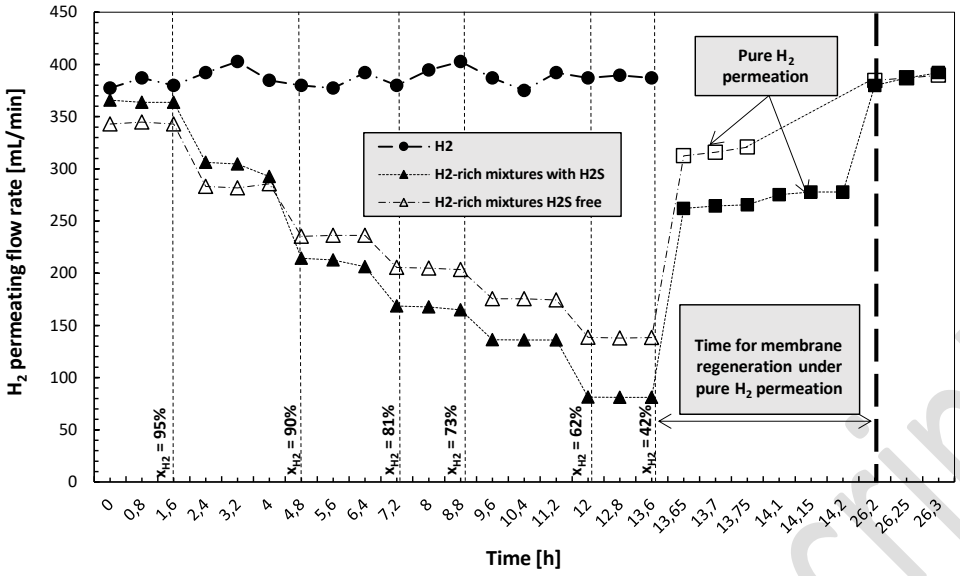

Figure 6. Volume flow rate permeating through the Pd-Au/Al_2O_3 membrane of H_2 as single gas and as component in H_2-rich gaseous mixtures (with and without H_2S) vs time at 673 K and 100 kPa of H_2 partial pressure difference across the membrane.

Figure 6 sketches a constant trend of the permeating volume flow rate of H_2 (around 380 mL/min as mean value) as single gas in a range time of 14 h under testing at 673 K and 100 kPa of H_2 partial pressure difference across the membrane. To evaluate the effects on the H_2 permeation of other compounds typically present in a SRB reformed streams (CO_2, CH_4, N_2, and H_2S), the two gaseous mixtures (with and without H_2S) were mixed with a constant H_2 stream and the H_2 partial pressure difference across the membrane was set at 100 kPa. This was done by varying the total feed pressure as a consequence of the H_2 composition variation in the final H_2-rich gas mixtures in order to be able to correctly compare the H_2 permeation through the membrane at the same H_2 partial pressure difference set for the case of H_2 tested as a single gas. Considering the H_2-rich gas mixture without H_2S, it is evident that the lower is the H_2 composition, the higher is the depletion of the H_2 permeating flow rate as a consequence of the ever more pronounced concentration polarization effect. Furthermore, as demonstrated by Mejdell et al. [71], the presence of a growing amount of CO_2 in the gaseous mixture is a further reason of the depletion of the H_2 permeating flow rate, since it may be adsorbed on the membrane surface, inducing an inhibitive effect on the H_2 permeation. Hence, the H_2 flow rate permeating through the Pd-Au/Al_2O_3 membrane ranged from 340 mL/min at x_{H2} = 0.95 to 140 mL/min at x_{H2} = 0.42. The initial H_2 permeation membrane performances were recovered reaching the permeating flow rate of 380

mL/min after 13 h of pure H_2 flowed as single gas into the MR module. However, the depletion of the H_2 permeating flow rate was more severe when H_2S was present in the H_2-rich gas mixture. A part from the aforementioned effects of the concentration polarization and CO_2 inhibition, the presence of H_2S lowered the H_2 permeating flow rate, which passed from 365 mL/min at x_{H2} = 0.95 to 81 mL/min at x_{H2} = 0.42. Even in this case, the H_2 permeation characteristics of the Pd-Au/Al_2O_3 membrane were reversibly recovered after flowing once again pure H_2 to the membrane module. The capacity of fully restoring the hydrogen permeation characteristics shown by the non-commercial membrane results to be one of the most significative results of this work because it avoids the substitution of the membrane, hence resulting economically attractive for possible scale up of this technology.

3.3 Preliminary experimental tests on the commercial self-supported Pd-Ag membrane: gas permeation analyses

The single gas permeation tests on the self-supported Pd-Ag membrane were performed at different temperatures ranging between 573 and 673 K, by varying the transmembrane pressure between 0 and 200 kPa, Figure 7(a). The maximum operating temperature for this commercial membrane is set at 673 K, consequently, all the experimental campaign considered the aforementioned temperature as the maximum operable condition. The experiments evidenced that only H_2 may permeate through the membrane for all the tested temperatures. Therefore, the H_2 permeation mechanism is regulated by the diffusion through the membrane bulk and the H_2 permeating flux followed the Sieverts-Fick law (n-value equal to 0.5). As for the supported Pd-Au/Al_2O_3 membrane, also for the self-supported Pd-Ag membrane the H_2 permeating flux increased as a consequence of both temperature and transmembrane H_2 partial pressure difference raise.

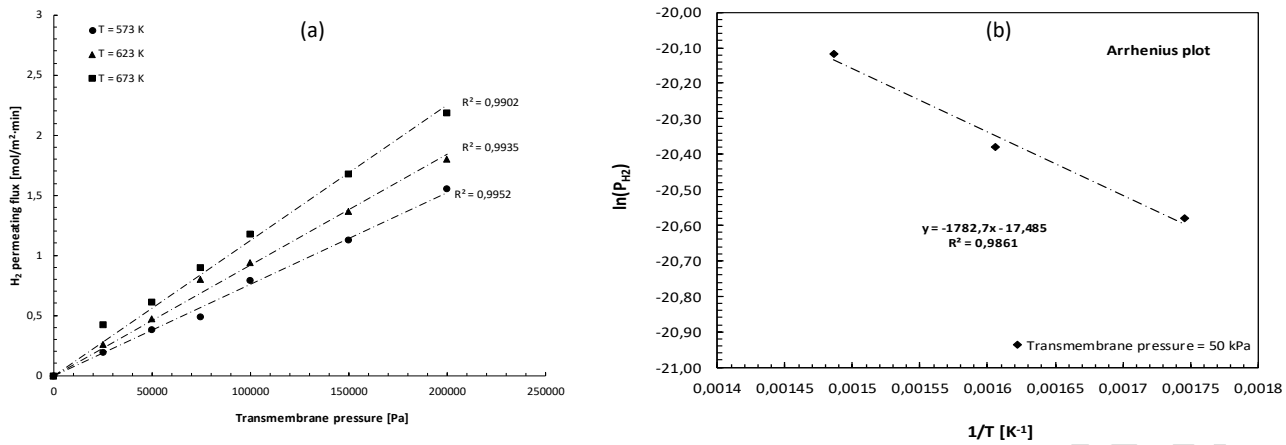

Figure 7. (a) H_2 flux permeating through the self-supported Pd-Ag membrane vs transmembrane pressure at different operating temperature; (b) H_2 permeability vs 1/T for the self-supported Pd-Ag membrane at 50 kPa of transmembrane pressure.

Figure 7(b) shows the Arrhenius plot for the Pd-Ag membrane at transmembrane pressure equal to 50 kPa. In this case, the apparent activation energy was equal to 14.8 kJ/mol.

3.4 SRB reaction tests

SRB reaction tests were carried out firstly in the Pd-Au/Al_2O_3 MR at 823 K and 150 kPa, by varying the H_2O/CH_4 molar ratio between 2/1 and 3/1, and the WHSV between 0.5 and 1.3 h^{-1}, analyzing the experimental results in term of CH_4 conversion, Figure 8(a) and H_2 recovery, Figure 8(b). As shown in Figure 8(a), at constant WHSV CH_4 conversion increased at a higher H_2O/CH_4 molar ratio (from 18 to almost 25% at WHSV = 0.5 h^{-1}) because, as expected, an excess of steam favored higher conversions from a thermodynamic point of view. Nevertheless, no higher feed molar ratios were used because a larger excess of steam may determine a negative effect on the H_2 permeation mechanism, acting a dilution of the products present in the reaction side, lowering the H_2 partial pressure and, consequently, the H_2 permeation driving force.

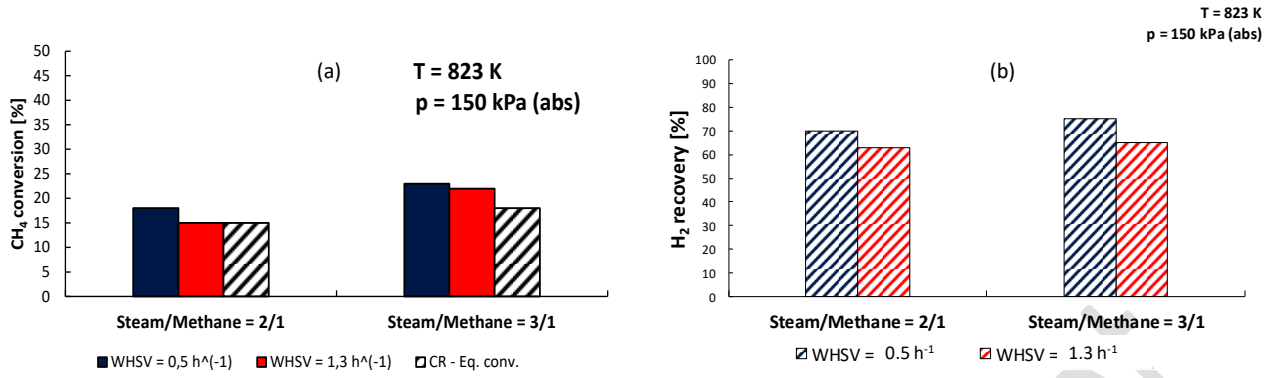

Figure 8. (a) CH_4 conversion vs feed molar ratio at different WHSV, T = 823 K and p = 150 kPa during SRB reaction carried out in the Pd-Au/Al_2O_3 MR in comparison with the equilibrium conversion at the set conditions in an equivalent CR; (b) H_2 recovery vs feed molar ratio at different WHSV, T = 823 K and p = 150 kPa during SRB reaction carried out in the Pd-Au/Al_2O_3 MR.

In comparison with an equivalent CR operated at the same experimental conditions, the Pd-Au/Al_2O_3 MR showed a better conversion at lower WHSV and stoichiometric feed molar ratio, whereas it was comparable at higher WHSV, Figure 8(a). On the contrary, in the presence of an excess of water in the feed, CH_4 conversion overcame the thermodynamic equilibrium conversion of the equivalent CR at both the WHSVs investigated in this work.

However, at each feed molar ratio, an increase of WHSV lowers the CH_4 conversion due to the lower contact time between the reactants and the catalyst, Figure 8(a). This involves a reduction of H_2 produced during the reaction and, consequently, a lower H_2 permeation driving force, responsible for a lower H_2 removal and, consequently, for a lower H_2 recovery, Figure 8(b). On the contrary, an increase of feed molar ratio induces an enhancement of H_2 production, involving a higher H_2 permeation driving force with a consequent larger H_2 removal from the reaction to the permeate side. This favors an increase of H_2 collected in the latter side and, consequently, the increment of the H_2 recovery (from 70 to almost 80% at WHSV = 0.5 h^{-1}), Figure 8(b). To confirm that coke was formed during the SRB reaction, after each experimental test, a H_2/N_2 mixture was fed to the reaction side of the MR in order to observe a possible formation of CH_4 as proof of its presence. No O_2 was used because it could oxidize the metallic layer of the membrane, causing its failure. In all the experimental tests, the GC analyses confirmed the production of CH_4, and the evolution of the depletion of the H_2 stream fed during the H_2/N_2 mixture treatment was detected up to completely convert the coke

present in the reaction zone. This objective was achieved when the H_2 molar flow rate fed to the MR (by using the H_2/N_2 mixture) was equal to that present in the outlet stream, as a proof that no C was present in the reaction side. As expected, more coke was formed at lower feed molar ratio and higher WHSV. In order to be sure about the validity of the experimental tests, the carbon balance within the inlet and outlet streams was evaluated also taking into account the amount of coke formed during the H_2/N_2 mixture treatment (this was done by integrating the evolution of the CH_4 molar flow rates detected during the H_2/N_2 treatment). The carbon balance was then closed in all the experimental tests with a maximum error equal to ±6%.

From a general point of view, although superior to the maximum conversions achievable in the equivalent CR at the same set conditions, the conversions of the Pd-Au/Al_2O_3 MR were limited by the relatively low H_2 perm-selectivity (as a consequence of the non-full H_2 perm-selectivity of this membrane), which did not allow to involve a stronger 'shift effect' of the SRB reaction system.

On the contrary, the experimental campaign using the self-supported Pd-Ag MR evidenced great performance in terms of conversion, although with limited H_2 recovery. Figure 9(a) shows the CH_4 conversion at 673 K as a function of reaction pressure and WHSV. The different reaction temperature at which the Pd-Ag MR was exercised with respect to the Pd-Au/Al_2O_3 MR was due to the maximum temperature limit imposed for avoiding the Pd-Ag membrane failure. As for the first MR, the conversion was improved by increasing the feed molar ratio and lowering the WHSV. As the best value, the Pd-Ag MR reached almost 85% of CH_4 conversion at 673 K, feed molar ratio = 3/1 and WHSV = 0.2 h^{-1}. Being the Pd-Ag membrane fully H_2 perm-selective, the shift effect operated by the membrane in removing H_2 from the reaction side to the permeate side was more effective, determining enhanced conversions with respect to the previous MR investigated. Figure 9(b) sketches the H_2 recovery against the feed molar ratio at 673 K, 100 kPa of transmembrane pressure and different WHSVs. Being the Pd-Ag membrane less permeable than the Pd-Au/Al_2O_3 membrane, the H_2 recovery during SRB reaction in the Pd-Ag MR was macroscopically lower than that achieved in the Pd-Au/Al_2O_3 MR. The best value, equal to almost 40%, was reached at feed molar ratio = 3/1 and WHSV = 0.2 h^{-1}.

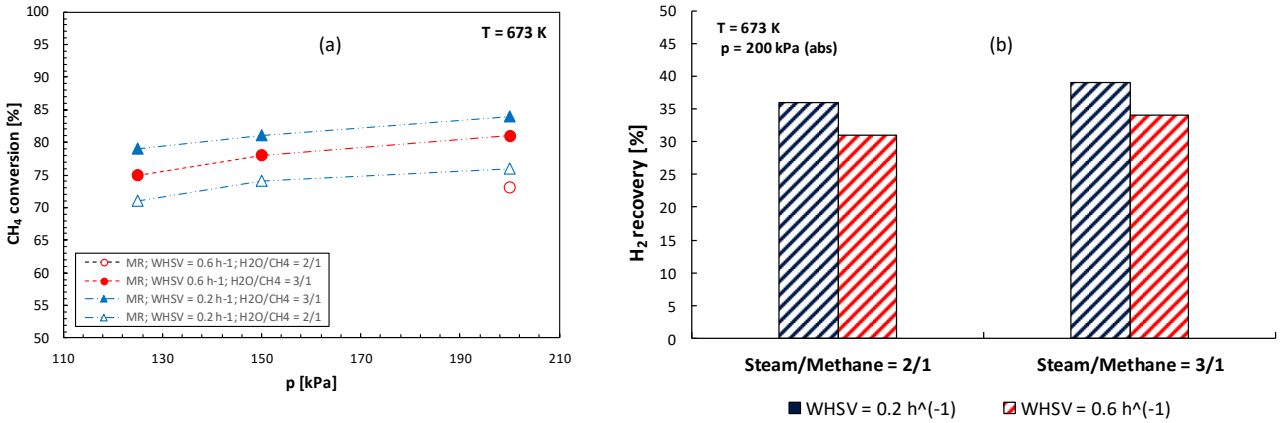

Figure 9. (a) CH_4 conversion vs feed molar ratio at T = 673 K and different reaction pressure and WHSV during SRB reaction carried out in the Pd-Ag MR; (b) H_2 recovery vs feed molar ratio at different WHSV, T = 673 K and p = 200 kPa during SRB reaction carried out in the Pd-Ag MR.

In Table 6, the best performance of the supported Pd-Au/Al_2O_3 and unsupported Pd-Ag MRs are reported. Much better CH_4 conversion was achieved in the Pd-Ag MR due to a large effect of the SRB reaction shift towards the products, as a consequence of the selective hydrogen permeation through the membrane. The former MR achieved great performance even though it was exercised at a lower temperature (673 K) and this constituted a further advantage over the Pd-Au/Al_2O_3 MR in terms of energy saving. However, due to the low hydrogen permeability characteristics of the unsupported Pd-Ag membrane related to its thick wall (150 μm) the hydrogen recovery was not higher than 40% although its purity was around 100% with a CO content $\leq$ 20 ppm, making this stream useful for low-temperature (LT) PEM fuel cell supplying. Nevertheless, the composition of hydrogen of the retentate stream is equal to a bit more than 50% at the best conditions Figure 10(a), decreasing to around 40% at lower H_2O/CH_4 molar ratio, Figure 10(b). Hence, the retentate stream would need to be treated in a second stage process to further transform the residual CH_4 into H_2 and CO_2 and recover as much as possible H_2, implying additional operation costs due to a higher number of stages processing.

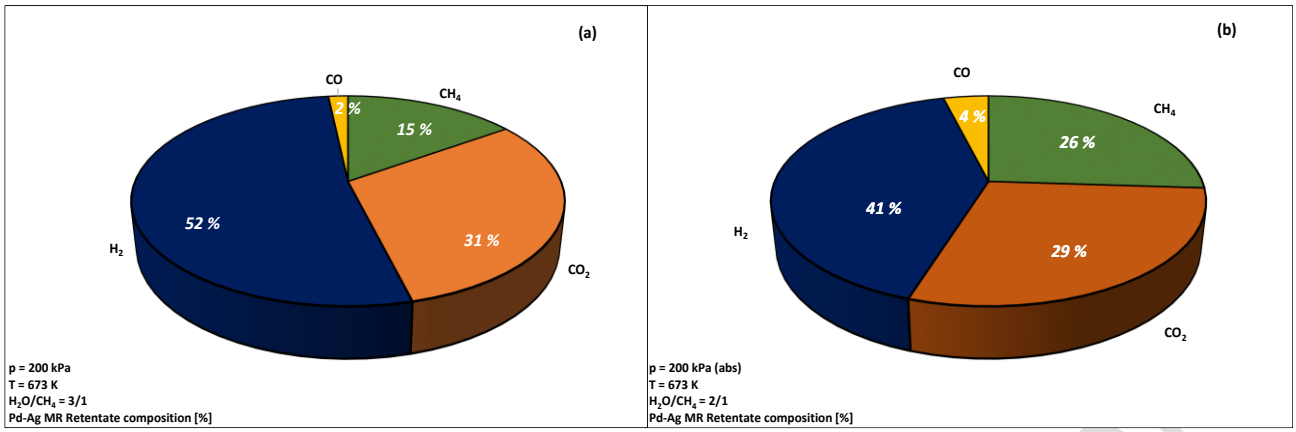

Figure 10. Molar retentate composition (dry) at WHSV = 0.2 h^{-1}, T = 673 K and p = 200 kPa during SRB reaction carried out in the Pd-Ag MR: (a) feed molar ratio = 3/1; (b) feed molar ratio = 2/1.

On the other hand, the Pd-Au/Al_2O_3 MR allowed higher hydrogen recovery (80% at the best conditions as reported in Table 6) with a purity not adequate to low-temperature PEM fuel cells supplying (CO content at the best operation conditions investigated in this work equal to 1300 ppm), but useful for feeding high-temperature PEM or other kinds of fuel cells.

Table 6. SRB reaction carried out in MRs and CRs. Qualitative comparison among the experimental results of this work and literature data.

Reactor typology	Membrane typology	Selective dense layer [μm]	Catalyst	T [K]	p [kPa]	H_2O/CH_4 feed ratio	CH_4 conversion [%]	H_2 recovery [%]	H_2 purity [%]	Ref.
MR[a]	Pd-Au/Al_2O_3	~ 8	Rh/$MgAl_2O_4$/Al_2O_3	823	150	3/1	25	~ 80	~ 50	**This work**
MR[b]	Pd-Au/Al_2O_3	~ 8	Rh/$MgAl_2O_4$/Al_2O_3	823	150	3/1	45	82	55	**This work**
MR[a]	Pd-Ag	150	Rh/$MgAl_2O_4$/Al_2O_3	673	200	3/1	85	~ 40	~ 100	**This work**
MR[b]	Pd-Ag	150	Rh/$MgAl_2O_4$/Al_2O_3	673	200	3/1	97	45	~ 100	**This work**
MR[b]	Pd-Ag	200	Ru/Al_2O_3	723	500	3/1	-	~ 10	~ 100	[32]
MR[b]	Pd-Ag	200	Ru/Al_2O_3	723	100	3/1	-	50	~ 100	[33]
MR[b]	Pd/Al_2O_3	7	Ni/Al_2O_3	723	350	3/1	34	70	70	[36]
MR[b]	Pd-Ag	~ 80	Ni/Al_2O_3	823	100	-	15	-	~ 100	[38]
CR[b]	-	-	Ni-Rh/Al_2O_3	973	120	3/1	85	-	~ 77[c]	[72]
CR[a]	-	-	Ni-Rh/Al_2O_3	973	120	3/1	~ 20	-	~ 20[c]	[72]
CR[b]	-	-	Ni/Al_2O_3	964	-	2/1	~ 85	-	58	[73]
CR[b]	-	-	Ni/CeO_2	873	-	1/1	58	-	59	[74]
CR[b]	-	-	Rh/CeO_2	1173		3/1	100	-	63	[75]
CR[b]	-	-	Ni/Al_2O_3	1073	100	2/1	99	-	45	[76]
CR[a]	-	-	Ni/Al_2O_3	1073	100	2/1	22	-	-	[76]

[a] H_2S in the feed

[b] H_2S free feed

[c] Calculated

Nevertheless, the low hydrogen perm-selectivity characteristics of the supported Pd-Au/Al_2O_3 membrane affected at lot the SRB reaction performance in terms of CH_4 conversion even though it was qualitatively

comparable with other few data about supported Pd-based MRs present in literature working at similar temperatures (Table 6), although the experimental data of this work dealt with a model biogas stream containing H_2S.

To evaluate the negative effect on the catalytic performance due to the presence of H_2S in the feed stream, a H_2S free model biogas stream (Table 5) was adopted to carry out the SRB reaction in both the MRs and the results were reported in Table 6. As shown, the Pd-Au/Al_2O_3 MR reached better CH_4 conversion (45%) at 823 K, 150 kPa of pressure and 3/1 as feed molar ratio than the case of supplying a model biogas stream containing H_2S (~ 25%). Meanwhile, both H_2 recovery (82%) and purity (55%) were slightly higher, probably due to the larger amount of H_2 present in the reaction side that globally enhanced the H_2 permeation driving force. Also in the case of the Pd-Ag MR, at 673 K, 200 kPa, and 3/1 as feed molar ratio, CH_4 conversion improved up to 97% as well as the H_2 recovered in the permeate side (45%). What reported above demonstrated that the presence of H_2S in the model biogas feed stream affected negatively the catalyst and membrane performance in both the MRs. This was also recently confirmed by Yin et al. [60], who carried out the SRB in a CR at 973 K, 120 kPa, and 3/1 as feed molar ratio, observing the CH_4 conversion decrease from 85% (in the case of a model H_2S free biogas stream supplying) to around 20% (using a model H_2S containing biogas stream), Table 6. In addition, Papurello et al. [64] observed lower catalytic performance during SRB in a CR exercised at 1073 K, 100 kPa and stoichiometric feed ratio owing to the negative effect of H_2S present in the model biogas feed stream, registering the depletion of CH_4 conversion from 99 to 22%.

To check the performance (in terms of CH_4 conversion) during SRB in both of the MRs under longer-term reaction tests, the operating conditions were set at 823 K, 150 kPa and feed molar ratio = 3/1 for the Pd-Au/Al_2O_3 MR and at 673K, 200 kPa and feed molar ratio = 3/1 for the Pd-Ag MR, supplying the synthetic biogas stream containing H_2S. As shown in Figure 11, in the first 50 minutes transient phenomena occurred, in which CH_4 conversion increased up to around 25-30% for the Pd-Au/Al_2O_3 MR and 85% for the Pd-Ag MR. Afterwards, the conversion remained stable in the first MR up to around 400 min; then, it slightly decreased up to less than 10% after 1000 min under testing. For the second MR, the conversion remained stable up to around 200 min; after that, it decreased quickly up to reach around 10% after 1000 min under testing.

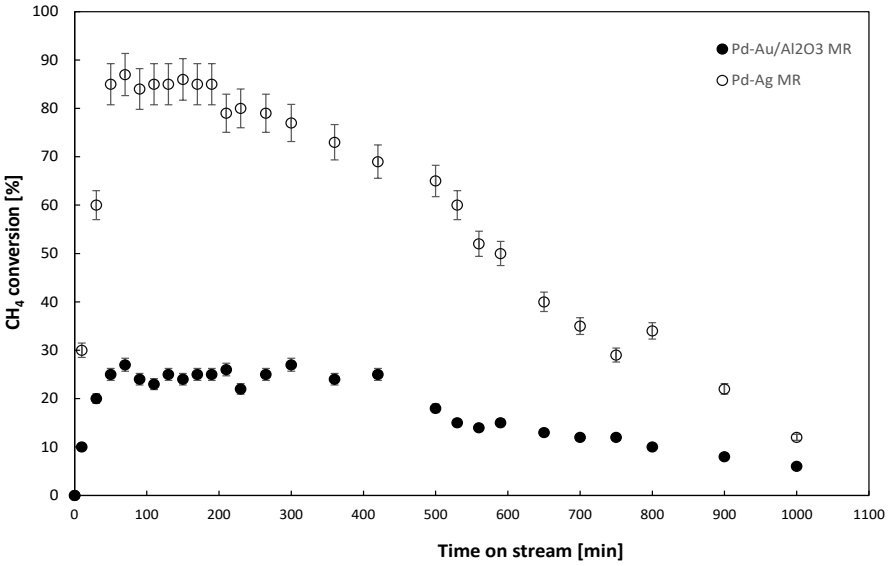

Figure 11. CH_4 conversion vs time on stream during SRB reaction in (a) Pd-Au/Al_2O_3 MR, (b) Pd-Ag MR. Experimental conditions: (a) T = 823 K, p = 150 kPa, feed molar ratio = 3/1; (b) T = 673, p = 200 kPa, feed molar ratio = 3/1. A synthetic H_2S containing biogas mixture was used as feed stream (Table 2).

Although qualitatively the Pd-Au/Al_2O_3 MR showed lower conversions than the Pd-Ag MR, it is possible to observe that the first MR contrasted better the exposure to the H_2S containing biogas feed stream, doubling the time in which a performance decrease was observed in the second MR. This could be due to the higher H_2S resistance of the Pd-Au alloy than the Pd-Ag one [65], making stable the performance of the Pd-Au/Al_2O_3 MR for a longer operation time.

3.4 Post mortem analyses

After the experimental campaign, a post mortem analysis was carried out on the supported Pd-Au/Al_2O_3 (non-commercial) membrane. The SEM images at different magnification of the upper part of the Pd-Au layer evidence still the typical cauliflower morphology, Figure 12(a), whereas EDX analysis pointed out the presence of sulfur as a consequence of a possible membrane surface contamination Figure 12(b), which could be responsible for the gradual decrease in the perm-selectivity characteristics of the membrane, Figure 6, and its deactivation in time, Figure 11.

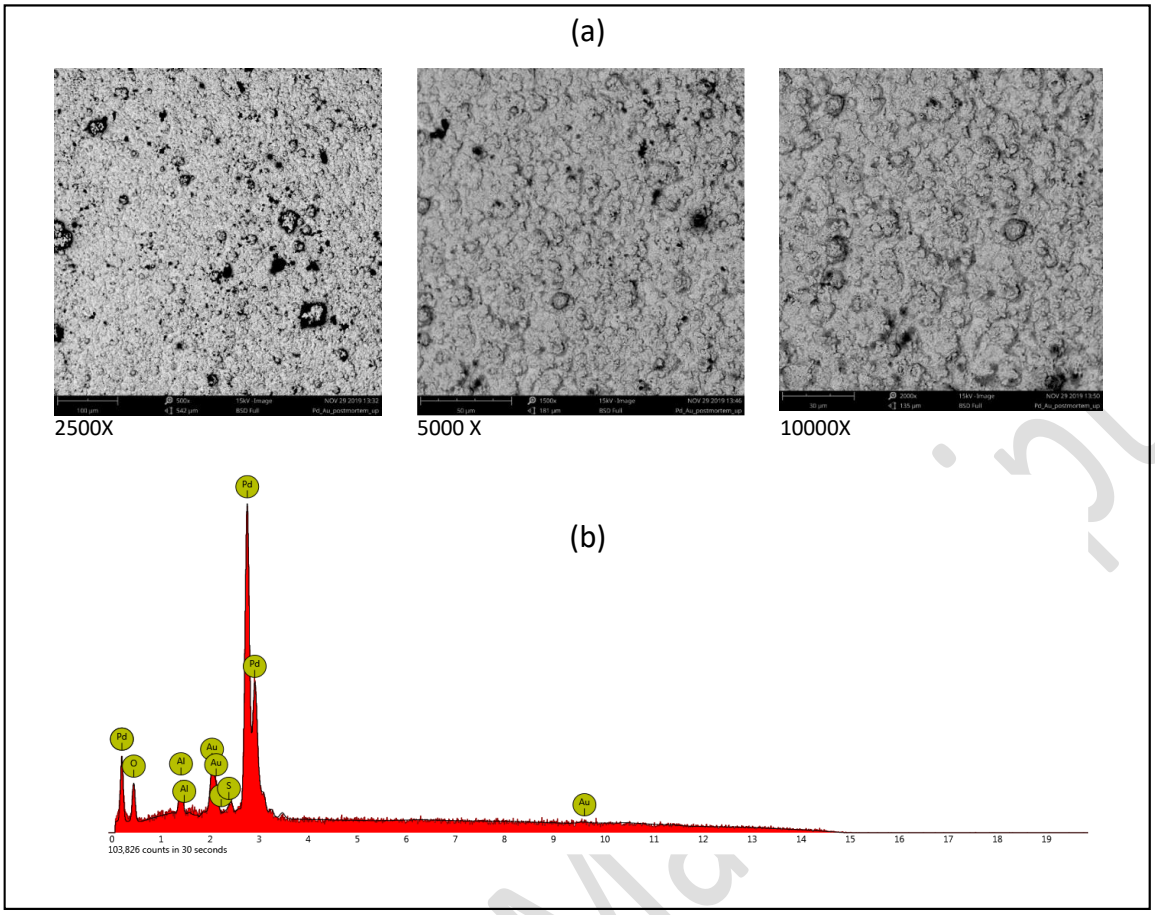

Figure 12. Post mortem analysis: (a) SEM images of the Pd-Au/Al_2O_3 membrane (outer) surface at different magnification and an accelerating voltage of 15 kV; (b) EDX analysis on the Pd-Au/Al_2O_3 membrane after the experimental campaign.

Conclusion

The steam reforming of a H_2S containing biogas mixture was carried out over a non-commercial Rh(1%)/$MgAl_2O_4$/Al_2O catalyst in two Pd-based MRs to evaluate the effects of the H_2S presence during the SRB reaction on the MRs performance in terms of hydrogen permeation characteristics and catalytic activity as the first time (to our best knowledge).

A high hydrogen permeable and low hydrogen perm-selective supported Pd-Au/Al_2O_3 membrane housed in a MR showed limited CH_4 conversion, around 25% (the best value), reached at 823 K and 150 kPa, but relatively high hydrogen recovery, 80%, reached at the same operating conditions. For comparison, feeding a H_2S free biogas mixture the conversion and hydrogen recovery were superior to the previous case (45% and 82%, respectively, at 823 K and 150 kPa), pointing out how the H_2S induced a depletion of the Pd-

Au/Al_2O_3 MR performance. A depletion of catalytic activity with time was also observed as there was a progressive decrease of CH_4 conversion, from 25-30% to less than 10%, under H_2S containing biogas stream conditions. As confirmed by the hydrogen-rich gas mixture (H_2S containing) permeation tests, the Pd-Au alloy seems to be more resistant to the H_2S attack than the Pd-Ag, even though the defects in the metallic layer of the supported $Pd\text{-}Au/Al_2O_3$ membrane limited the performance in terms of hydrogen perm-selectivity. Furthermore, as evidenced by the EDX tests in the post mortem analyses, the presence of sulfur was detected in the Pd-Au metallic layer. Nevertheless, the hydrogen permeation characteristics of the $Pd\text{-}Au/Al_2O_3$ membrane were recovered by feeding pure hydrogen allowing its utilization in other experimental campaigns.

The utilization of a low permeable but fully hydrogen perm-selective Pd-Ag membrane (commercial) in a MR allowed better performance than the previous MR in terms of conversion, 85%, reached at milder operating temperature (673 K). It was due to the larger shift effect realized by the fully hydrogen perm-selective Pd-Ag membrane on the SRB reaction system with the further advantage of recovering a pure hydrogen stream. On the contrary, owing to the thicker metallic layer, the hydrogen permeability was relatively low and the hydrogen recovered was not higher than 40% at 673 K and 200 kPa.

Under long-term SRB reaction tests, the Pd-Ag MR showed a faster decrease of the CH_4 conversion (from 85 to around 10%) than the $Pd\text{-}Au/Al_2O_3$ MR due to the effect of H_2S present in the biogas feed mixture because - as also confirmed in the specialized literature ([44-46]) - the Pd-Au alloy seems to be more H_2S resistant than other Pd-alloys. Furthermore, the negative effect of H_2S was permanent in the Pd-Ag membrane, determining its failure after a prolonged exposure, which was not recovered by supplying pure hydrogen as in the case of the supported Pd-Au membrane of this work.

As a future work, a better deposition of the metallic layers (Pd and Au) on the Al_2O_3 support will constitute the future development of this kind of supported membrane in order to improve its hydrogen perm-selectivity and, consequently, the conversion and hydrogen permeation performance during the steam reforming of biogas mixtures (*in natura*).

Acknowledgments

Nanjing Tech. University & GaoQ Functional Materials Co., Ltd. (China) are particularly acknowledged for providing the Pd-Au/α-Al_2O_3 membrane used in this work.

Acronyms

CR	Conventional Reactor
EDX	Energy Dispersive X-ray
GC	Gas Chromatograph
WHSV	Weight Hourly Space Velocity
HT	High Temperature
LT	Low Temperature
MR	Membrane Reactor
PEM	Proton Exchange Membrane
SEM	Scanning Electron Microscopy
SRB	Steam Reforming of Biogas

Symbols

E_A	Apparent activation energy
$F_{permeate}$	Outlet permeate molar flow rate
$H_{2\text{-permeate}}$	Permeate H_2 molar flow rate
$H_{2\text{-retentate}}$	Retentate H_2 molar flow rate
J_{H2}	H_2 permeating Flux
n	Dependence factor of the hydrogen flux on the hydrogen partial pressure
Pe	H_2 permeance
P_{H2}	H_2 permeability
$P_{H2,0}$	Pre-exponential factor
$p_{H2\text{-permeate}}$	H_2 partial pressures in the permeate side
$p_{H2\text{-retentate}}$	H_2 partial pressures in the retentate side
R	The universal gas constant,
T	Temperature.
Δp	Transmembrane pressure
$\alpha_{H2/i}$	Ideal selectivity of H_2 over another gas

References

[1] Y. Kalmykova, M. Sadagopan, L. Rosado, Circular economy – From review of theories and practices to development of implementation tools, Resou. Conserv. Recycl., 135 (2018) 190-201.
[2] K. Handayani, Y. Krozer, T. Filatova, From fossil fuels to renewables: An analysis of long-term scenarios considering technological learning, Energy Policy, 127 (2019) 134-146.
[3] A. Górak, A. Stankiewicz (Eds.). (2011). Research Agenda for Process Intensification: Towards a Sustainable World of 2050. Creative Energy - Energy Transition. Retrieved from http://3me.tudelft.nl/fileadmin/Faculteit/3mE/Actueel/Nieuws/2011/docs/DSD_Research_Agenda.pdf (Accessed July 2020).
[4] K.K. Sirkar, A.G. Fane, R. Wang, R. Wickramasinghe, Process intensification with selected membrane processes, Chem. Eng. Proce. Process Int., 87 (2015) 16-25.

[5] E. Drioli, A. Brunetti, G. Di Profio, G. Barbieri, Process intensification strategies and membrane engineering, Green Chem., 14 (2012) 1561-1572.
[6] T. Biegler, The hydrogen economy, The Skeptic, 25 (2005) 1-29.
[7] N. Armaroli, V. Balzani, The Hydrogen Issue, ChemSusChem. 4 (2011) 21–36.
[8] A. Górak, A. Stankiewicz (Eds.). (2011). Research Agenda for Process Intensification: Towards a Sustainable World of 2050. Creative Energy - Energy Transition. Retrieved from http://3me.tudelft.nl/fileadmin/Faculteit/3mE/Actueel/Nieuws/2011/docs/DSD_Research_Agenda.pdf (Accessed July 2020).
[9] US Department of Energy. Hydrogen production pathways (2017). Website: http://energy.gov/eere/fuelcells/hydrogen-production-pathways (Accessed September 2019).
[10] M. Van der Hoeven, Technology Road Map: Hydrogen and Fuel Cells - International Energy Agency (2015) 1-75.
https://www.iea.org/publications/freepublications/publication/TechnologyRoadmapHydrogenandFuelCells.pdf (Accessed July 2020).
[10] M. Voldsund, K. Jordal, R. Anantharaman, Hydrogen production with CO_2 capture, Int. J. Hydrogen Energy. 41 (2016) 4969-4992.
[11] Y.F. Yan, L. Zhang, L.X. Li, Q. Tang, Progress in catalytic membrane reactors for high purity hydrogen production, J. Inorg. Mater., 26 (2011) 1233-1243.
[12] A. Iulianelli, A. Basile, New perspectives in hydrogen production, separation and utilization, in Current Trends and Future Developments on (Bio-) Membranes series, ISBN 9780128173848, Elsevier Publishing, 2020, pp. 1-462. https://www.elsevier.com/books/current-trends-and-future-developments-on-bio-membranes/basile/978-0-12-817384-8.
[13] A. Brunetti, P. Zito, L. Giorno, E. Drioli, G. Barbieri, Membrane reactors for low temperature applications: An overview, Chem. Eng. Proc. Process Intensif., 124 (2018) 282-307.
[14] M. Meénendez, Inorganic membrane reactors for energy applications, Nanoporous Materials for Energy and the Environment, Pan Stanford Publishing Pte. Ltd., G. Rios, G. Centi, N. Kanellopoulos (Eds.), ISBN 978-981426717-5, (2011), pp. 283-297.
[15] A. Iulianelli, S. Liguori, A. Vita, C. Italiano, C. Fabiano, Y. Huang, A. Basile, The oncoming energy vector: hydrogen produced in Pd-composite membrane reactor via bioethanol reforming over Ni/CeO_2 catalyst, Catal. Today, 259 (2016) 368-375.
[16] A. Iulianelli, A. Basile, Development of membrane reactor technology for H_2 production in reforming process for low-temperature fuel cells, Ch. 12 in Current Trends and Future Developments on (Bio-) Membranes: Co-generation systems and membrane technology (A. Basile Ed.), ISBN: 978-0-12-817807-2, Elsevier (2020), pp. 287-305.
[17] N.Z. Muradov, N.T. Veziröglu, From hydrocarbon to hydrogen-carbon to hydrogen economy. Int. J. Hydrogen En., 30 (2005) 225-237.
[18] ISO 14001:2015 Environmental management systems — Requirements with guidance for use, 3 (2015) 1-35, https://www.iso.org/standard/60857.html (Accessed on July, 2020)
[19] European Industrial Gases Association (EIGA) Doc. 122/18, Environmental impact of hydrogen plants, https://www.eiga.eu/index.php?eID=dumpFile&t=f&f=3445&token=0c6c43064280cb30331fe047f6b798485b157e2a (Accessed on July, 2020).
[20] A. Brunetti, Y. Sun, A. Caravella, E. Drioli, G. Barbieri, Process intensification for greenhouse gas separation from biogas: More efficient process schemes based on membrane-integrated systems, Int. J. Greenhouse Gas Contr., 35 (2015) 18-29.
[21] C.S. Lau, A. Tsolankis, M.L. Wyszynski, Biogas upgrade to syn-gas (H_2-CO) via dry and oxidative reforming, Int. J. Hydrogen En., 36 (2011) 397-404.
[22] S. Rasi, A. Veijanen, J. Rintala, Trace compounds of biogas from different biogas production plants, Energy, 32 (2007) 1375-1380.
[23] S.D. Angeli, L. Turchetti, G. Monteleone, A.A. Lemonidou, Catalyst development for steam reforming of methane and model biogas at low temperature, Appl. Catal. B Env., 181 (2016) 34-46.
[24] S. Araki, N. Hino, T. Mori, S. Hikazudani, Durability of a Ni based monolithic catalyst in the autothermal reforming of biogas, Int. J. Hydrogen En., 34 (2009) 4727-4734.

[25] M. Luneau, E. Gianotti, F.C. Meunier, C. Mirodatos, E. Puzenat, Y. Schuurman, N. Guilhaume, Deactivation mechanism of Ni supported on Mg-Al spinel during autothermal reforming of model biogas, Appl. Catal. B Env., 203 (2017) 289-299.
[26] J. Xu, W. Zhou, Z. Li, J. Wang, J. Ma, Biogas reforming for hydrogen production over a Ni–Co bimetallic catalyst: Effect of operating conditions, Int. J. Hydrogen En., 35 (2010) 13013-13020.
[27] S. Damyanova, B. Pawelec, K. Arishtirova, J.L.G. Fierro, Biogas reforming over bimetallic PdNi catalysts supported on phosphorus-modified alumina, Int. J. Hydrogen En., 36 (2011) 10635-10647.
[28] U. Izquierdo, V.L. Barrio, K. Bizkarra, A.M. Gutierrez, J.R. Arraibi, L. Gartzia, J. Bañuelos, I. Lopez-Arbeloa, J.F. Cambra, Ni and Rh single bond Ni catalysts supported on Zeolites L for hydrogen and syngas production by biogas reforming processes, Chem. Eng. J., 238 (2014) 178-188.
[29] N. Bion, D. Duprez, F. Epron, Design of nanocatalysts for Green hydrogen production from bioethanol, ChemSusChem, 5 (2012) 76-84.
[30] A. Le Valant, A. Garron, N. Bion, D. Duprez, F. Epron, Effect of higher alcohols on the performances of a 1%Rh/$MgAl_2O_4$/Al_2O_3 catalyst for hydrogen production by crude bioethanol steam reforming, Int. J. Hydrogen En., 36 (2011) 311-318.
[31] P. Durán, A. Sanz-Martínez, J. Soler, M. Menéndez, J. Herguido, Pure hydrogen from biogas: Intensified methane dry reforming in a two-zone fluidized bed reactor using permselective membranes, Chem. Eng. J., 370 (2019) 772-781.
[32] J.M. Vásquez Castillo, T. Sato, N. Itoh, Effect of temperature and pressure on hydrogen production from steam reforming of biogas with Pd-Ag membrane reactor, Int. J. Hydrogen En., 40 (2015) 3582-3591.
[33] T. Sato, T. Suzuki, M. Aketa, Y. Ishiyama, K. Mimura, Steam reforming of biogas mixtures with a palladium membrane reactor system, Chem. Eng. Sci., 65 (2010) 451-457.
[34] T.M. Raybold, M.C. Huff, Analyzing enhancement of CO_2 reforming of CH_4 in Pd membrane reactors, Aiche J., 48 (2002) 1051-1061.
[35] G. Di Marcoberardino, X. Liao, A. Dauriat, M. Binotti, G. Manzolini, Life cycle assessment and economic analysis of an innovative biogas membrane reformer for hydrogen production, Processes, 7 (2019) 86.
[36] A. Iulianelli, S. Liguori, Y. Huang, A. Basile, Model biogas steam reforming in a thin Pd-supported membrane reactor to generate clean hydrogen for fuel cells, J. Power Sou., 273 (2015) 25-32.
[37] D Saebea, S. Authayanun, Y. Patcharavorachot, A. Arpornwichanop, Enhancement of hydrogen production for steam reforming of biogas in fluidized bed membrane reactor, Chem. Eng. Trans., 39 (2014) 1177-1182.
[38] F.S.A. Silva, M. Benachour, C.A.M. Abreu, Evaluating hydrogen production in biogas reforming in a membrane reactor, Braz. J. Chem. Eng., 32 (2015) 201-210.
[39] G. Bagnato, A. Iulianelli, A. Vita, C. Italiano, M. Laganà, C. Fabiano, C. Rossi, A. Basile, Pure hydrogen production from steam reforming of bio-sources, Int. J. Membrane Sci. Techn., 2 (2015) 48-56.
[40] H.J. Alves, C.B. Junior, R.R. Niklevicz, E.P. Frigo, M.S. Frigo, C.H. Coimbra-Arau´ jo, Overview of hydrogen production technologies from biogas and the applications in fuel cells, Int. J. Hydrogen En., 38 (2013) 5215-5225.
[41] I.U. Khan, M.H. Dzarfan Othman, H. Hashim, T. Matsuura, A.F. Ismail, M. Rezaei-DashtArzhandi, I. Wan Azelee, Biogas as a renewable energy fuel – A review of biogas upgrading, utilization and storage, En. Conv. Managm., 150 (2017) 277-294.
[42] G. Di Marcoberardino, S. Foresti, M. Binotti, G. Manzolini, Potentiality of a biogas membrane reformer for decentralized hydrogen production, Chem Eng. Proc. Process Int., 129 (2018) 131-141.
[43] F. Braun, A.M. Tarditi, J.B. Miller, L.M. Cornaglia, Pd-based binary and ternary alloy membranes: Morphological and perm-selective characterization in the presence of H_2S, J. Membrane Sci., 450 (2014) 299-307.
[44] C.-H. Chen, Y.H. Ma, The effect of H_2S on the performance of Pd and Pd/Au composite membrane, J. Membrane Sci., 362 (2010) 535-544.
[45] A. Caravella, N. Hara, H. Negishi, S. Hara, Quantitative contribution of non-ideal permeability under diffusion-controlled hydrogen permeation through Pd-membranes, Int. J. Hydrogen En., 39 (2014) 4676-4682.

[46] S.-E. Nam, K.-H. Lee, Hydrogen separation by Pd alloy composite membranes: introduction of diffusion barrier, J. Membrane Sci., 192 (2001) 177-185.
[47] Z. Wang, V. Li, S.L.-I. Chan, Review of alloy membranes/films for hydrogen separation or purification, J. Rare Earths, 23 (2005) 611-616.
[48] M.R. Rahimpour, F. Samimi, A. Babapoor, T. Tohidian, S. Mohebi, Palladium membranes applications in reaction systems for hydrogen separation and purification: A review, Chem. Eng. Proc.: Proc. Intens., 121 (2017) 24-49.
[49] K.E. Coulter, J.D. Way, S.K. Gade, S. Chaudhari, G.O. Alptekin, S.J. DeVoss, S.N. Paglieri, B. Pledger, Sulfur tolerant PdAu and PdAuPt alloy hydrogen separation membranes, J. Membrane Sci., 405-406 (2012) 11-19.
[50] K. Zhang, J.D. Way, Palladium-copper membranes for hydrogen separation, Sep. Purif. Techn., 186 (2017) 39-44.
[51] S.W. Lee, D.K. Oh, J.W. Park, C.B. Lee, D.W. Lee, J.S. Park, S.H. Kim, K.R. Hwang, Effect of a Pt-ZrO_2 protection layer on the performance and morphology of Pd-Au alloy membrane during H_2S exposure, J. Alloys Compd., 641 (2015) 210–215.
[52] B.C. Nielsen, Ö.N. Dog˘an, B.H. Howard, Effect of temperature on the corrosion of Cu-Pd hydrogen separation membrane alloys in simulated syngas containing H_2S, Corrosion Sci., 96 (2015) 74-86.
[53] E. Acha, Y.C. van Delft, J.F. Cambra, P.L. Arias, Thin PdCu membrane for hydrogen purification from in-situ produced methane reforming complex mixtures containing H_2S, Chem. Eng. Sci., 176 (2018) 429-438.
[54] F. Braun, J.B. Miller, A.J. Gellman, A.M. Tarditi, B. Fleutot, P. Kondratyuk, L.M. Cornaglia, PdAgAu alloy with high resistance to corrosion by H_2S, Int. J. Hydrogen En., 37 (2012) 18547-18555.
[55] L.F. Zhao, A. Goldbach, H. Xu, Tailoring palladium alloy membranes for hydrogen separation from sulfur contaminated gas streams, J. Membrane Sci., 507 (2016) 55-62.
[56] A.E. Lewis, H. Zhao, H. Syed, C.A. Wolden, J. Douglas Way, PdAu and PdAuAg composite membranes for hydrogen separation from synthetic water-gas shift streams containing hydrogen sulfide, J. Membrane Sci., 465 (2014) 167-176.
[57] A. Iulianelli, J.C. Jansen E. Esposito, M. Longo, F. Dalena, A. Basile, Hydrogen permeation and separation characteristics of a thin Pd-Au/Al_2O_3 membrane: The effect of the intermediate layer absence, Catal. Today, 330 (2019) 32-38.
[58] A. Iulianelli, M. Alavi, G. Bagnato, S. Liguori, J. Wilcox, M.R. Rahimpour, R. Eslamlouyan, B. Anzelmo, A. Basile, Supported Pd-Au membrane reactor for hydrogen production: membrane preparation, characterization and testing, Molecules, 21 (2016) 581-594.
[47] **[59]** F. Auprêtre, C. Descorme, D. Duprez, D. Casanave, D. Uzio, Ethanol steam reforming over $Mg_xNi_{1-x}Al_2O_3$ spinel oxide-supported Rh catalysts, J. Catal., 233 (2005) 464-477.
[60] S.-K. Ryi, J.-S. Park, K.-R. Hwang, D.-W. Kim, H.-S. An, Pd-Cu alloy membrane deposited on alumina modified porous nickel support (PNS) for hydrogen separation at high pressure, Korean J. Chem. Eng., 29 (2012) 59-63.
[61] A. Iulianelli, K. Ghasemzadeh, M. Marelli, C. Evangelisti, A supported Pd-Cu/Al_2O_3 membrane from solvated metal atoms for hydrogen separation/purification, Fuel Proc. Techn., 195 (2019) 106141-106149.
[62] Neil S. Patki, Sean-Thomas B. Lundin, J. Douglas Way, Apparent activation energy for hydrogen permeation and its relation to the composition of homogeneous PdAu alloy thin-film membranes, Sep. Pur. Techn., 191 (2018) 370-374.
[63] M.S. Islam, M.M. Rahman, S. Ilias, Characterization of Pd-Cu membranes fabricated by surfactant induced electroless plating (SIEP) for hydrogen separation, Int. J. Hydrogen En., 37 (2012) 3477-3490.
[64] J.R. Brenner, G. Bhagat, P. Vasa, Hydrogen purification with palladium and palladium alloys on porous stainless steel membranes, Int. J. Oil Gas Coal Techn., 1 (2008) 109.
[65] W. Wang, X. Pan, X. Zhang, W. Yang, G. Xiong, The effect of co-existing nitrogen on hydrogen permeation through thin Pd composite membranes, Sep. Pur. Techn., 54 (2007) 262-271.
[66] S. Liguori, A. Iulianelli, F. Dalena, P. Pinacci, F. Drago, M. Broglia, Y. Huang, A. Basile, Performance and long-term stability of Pd/PSS and Pd/Al_2O_3 for hydrogen separation, Membranes, 4 (2014) 143-162.
[67] W.-H. Chen, M.-H. Hsia, Y.-H. Chi, Y.-L. Lin, C.-C. Yang, Polarization phenomena of hydrogen-rich gas in high-permeance Pd and Pd-Cu membrane tubes, Appl. Energy, 113 (2014) 41-50.

[68] N. Pomerantz, Y.H. Ma, Novel method for producing high H_2 permeability Pd membranes with a thin layer of the sulfur tolerant Pd/Cu fcc phase, 370 (2011) 97-108.
[69] S. Yun, S.T. Oyama, Correlations in palladium membranes for hydrogen separation: A review, J. Membrane Sci., 375 (2011) 28-45.
[70] A. Caravella, F. Scura, G. Barbieri, E. Drioli, Sieverts law empirical exponent for Pd-based membranes: critical analysis in pure H_2 permeation, J. Phys. Chem. B, 114 (2010) 6033-6047.
[71] A.L. Mejdell, M. Jøndahl, T.A. Peters, R. Bredesen, H.J. Venvik, Effects of CO and CO_2 on hydrogen permeation through a ~3 µm Pd/Ag 23 wt.% membrane employed in a microchannel membrane configuration, Sep. Purif. Techn., 68 (2009) 178-184.
[72] W. Yin, N. Guilhaume, Y. Schuurman, Model biogas reforming over Ni-Rh/$MgAl_2O_4$ catalyst. Effect of gas impurities, Chem. Eng. J., 398 (2020) 125534.
[73] A. Effendi, Z.-G. Zhang, K. Hellgardt, K. Honda, T. Yoshida, Steam reforming of a clean model biogas over Ni/Al_2O_3 in fluidized- and fixed-bed reactors, Catal. Today, 77 (2002) 181-189.
[74] H.S. Roh, I.H. Eum, D.W. Jeong, Low temperature steam reforming of methane over Ni–Ce(1−x)Zr(x)O2 catalysts under severe conditions, Renew. Ener., 42 (2012) 212-216.
[75] C. Italiano, M.A. Ashraf, L. Pino, C.W. Moncada Quintero, S. Specchia, A. Vita, Rh/CeO_2 thin catalytic Layer deposition on alumina foams: catalytic performance and controlling regimes in biogas reforming processes, 8 (2018) 448.
[76] D. Papurello, V. Chiodo, S. Maisano, A. Lanzini, M. Santarelli, Catalytic stability of a Ni-Catalyst towards biogas reforming in the presence of deactivating trace compounds, Renew. Ener., 127 (2018) 481-494.
[77] A Doukelis, K Panopoulos, A Koumanakos, E Kakaras, Fabrication of palladium-based membranes by magneton sputtering, Ch. 2 In Palladium membrane technology for hydrogen production, carbon capture and other applications: Principles, Energy Production and Other Applications, Woodhead Publishing Series in Energy, 2014, ISBN: 9781782422341, pp. 1-402.